

Uplink Transmission Design for Fluid Antenna-Enabled Multiuser MIMO Systems with Imperfect CSI

Linyue Hu, Luchu Li, Cunhua Pan, *Senior Member, IEEE*, Hong Ren, *Member, IEEE*

Abstract—This paper investigates a two-timescale uplink transmission framework for a fluid antenna-enabled multiuser multi-input multi-output system (MIMO-FAS). Antenna positions are optimized based on statistical channel state information (CSI), while beamforming vectors at the base station (BS) adapt to instantaneous CSI. Under a Rician fading channel with imperfect CSI, we establish a linear minimum mean square error (LMMSE)-based channel estimation approach and derive a closed-form expression for the achievable uplink rate using a low-complexity maximal-ratio-combining (MRC) detector. The optimization problem is formulated as a minimum user rate maximization problem by optimizing the fluid antenna positions, subject to the feasible region and the minimum spacing distance constraints. To address this non-convex problem, a genetic algorithm (GA) method is proposed, encoding antenna configurations as population individuals. Additionally, an accelerated gradient ascent algorithm is proposed to enhance computational efficiency. Numerical results validate the mathematical derivations and demonstrate that the proposed two-timescale transmission strategy significantly outperforms traditional FPA systems, with both algorithms achieving enhanced gains.

Index Terms—Fluid antenna system (FAS), two-timescale transmission design, antenna position optimization, MIMO, channel estimation.

I. INTRODUCTION

OVER the past decades, wireless communication technologies have evolved in response to the escalating demands for low-latency and high-capacity services [1]. As a cornerstone of modern wireless communication, multiple-input multiple-output (MIMO) provides enhanced spectral efficiency and reliability through beamforming gain, spatial multiplexing and diversity gains [2]. To date, MIMO technology has developed rapidly, transitioning from single-user MIMO (SU-MIMO) to multiuser MIMO (MU-MIMO), and more recently to massive MIMO. Nevertheless, prohibitive hardware costs and energy consumption associated with large-scale antenna arrays impede sustainable deployment for massive MIMO [3], [4]. Furthermore, conventional MIMO systems relying on fixed-position antennas (FPAs) suffer from static spatial configurations with limited degrees of freedom (DoFs) that fail to adapt to dynamic user distributions and time-varying channel conditions, thereby constraining the overall performance of the system.

To address these limitations, fluid antenna system (FAS), alternatively termed movable antenna (MA), has garnered considerable attention for its potential to overcome the challenge of FPAs. As a novel paradigm characterized by position and shape flexibility, FAS leverages advanced reconfigurable antenna technologies, including reconfigurable radio-frequency pixel arrays [5], liquid-based antennas [6], and motorized mechanical movable antennas [7]. In contrast to traditional FPA systems, FAS allows for dynamic repositioning of antennas within a predefined region, introducing additional DoFs in the physical layer. Notably, [8] has demonstrated that FAS can achieve spatial diversity with a single antenna, making it particularly suitable for size-constrained mobile devices. By enabling antennas' movement to cope with user distribution and channel conditions, FAS alleviates issues associated with FPAs that struggle to make full use of spatial diversity and multiplexing, thereby enhancing network capacity and reliability [9]. Furthermore, the fluid antenna can be repositioned from interference-prone areas to locations with more favorable channel conditions, facilitating efficient interference management without the need for additional antennas [10].

Initial FAS investigations focused on single-input single-output (SISO) systems, establishing theoretical foundations through outage probability analysis of single-antenna FAS [11] and demonstrating comparable capacity with multi-antenna systems [12]. Motivated by these works, researchers have devoted considerable efforts to studying FAS, ranging from performance analysis to channel estimation. [13] provided a closed-form expression of the average level crossing rate in FAS, [14] analyzed the FAS performance over general correlated channels, [15] proposed a novel sequential linear minimum mean-squared error (LMMSE)-based channel estimation method for a small number of fluid antenna ports, [16] studied the achievable performance of FAS when multiple ports could be active, and [17] developed a switched combining (SDC) scheme for FAS to reduce channel estimation overhead. A recent review has summarized literature related to FAS [18]. Several researches further indicated that the priority of hybrid architectures combining FAS with physical layer security [19], integrated sensing and communication (ISAC) [20] [21], and reconfigurable intelligent surfaces (RISs) [22].

Recent advancements further studied the FAS-enhanced MIMO (MIMO-FAS) system. To fully unleash the potential of MIMO-FAS, several works focused on antenna position optimization. [23] explored the optimal diversity and multiplexing tradeoff of MIMO-FAS to reveal the fundamental

Linyue Hu is with the College of Electronics and Information Engineering, Sichuan University, Chengdu 610065, China. (e-mail: hulyue@163.com)

Luchu Li, Cunhua Pan and Hong Ren are with National Mobile Communications Research Laboratory, Southeast University, Nanjing 211189, China. (e-mail: 220240860, cpan, hren@seu.edu.cn)

limits by optimizing antenna position, which can also be viewed as optimizing the ports. Expanding on this concept, [24] developed a new MA-enabled MIMO, which is effectively a MIMO-FAS, demonstrating that flexible antenna positioning enhances MIMO capacity by reconfiguring the channel between transceivers. Furthermore, the authors in [25] investigated uplink transmission where each user is equipped with a single fluid antenna, and minimized the total transmit power of all users by jointly optimizing each user's antenna position and the base station (BS) receive beamforming matrix. Further advancing the application of fluid antennas, [26] proposed a new BS architecture employing multiple fluid antennas in uplink transmission. Additionally, [27] jointly optimized transmitted power and antenna positions in a cell-free massive MIMO system with fluid antennas at access points to maximize the minimum uplink rate across users. At the same time, various optimization algorithms, including the alternating optimization (AO) algorithm in [24], [27] and particle swarm optimization (PSO) algorithm in [26], have been proposed and validated their effectiveness.

However, prevailing FAS studies rely critically on two fundamental yet impractical assumptions. The first is the availability of perfect instantaneous channel state information (CSI), while the second is the requirement for real-time adjustment of antenna positions. In practice, due to the fact that the frequent updates of antenna positions in each channel coherence time, the instantaneous CSI changes too rapidly to be reliably obtained, especially in fast-fading channel [15], [28]. On the other hand, mechanical latency in fluid antenna relocation hinders its adaptability to dynamical channel variations, posing a challenge for FAS in fast-moving transceiver locations [29].

To address these two practical challenges, some researchers considered the use of statistical CSI for antenna position optimization [30], [31], [32]. In [31], the authors developed a rate maximization framework for transmit precoding and transmit/receive fluid antenna position designs with statistical CSI in the MIMO-FAS system. [32] introduced a two-timescale downlink transmission framework for MIMO-FAS with perfect CSI. In the two-timescale scheme, the beamforming vectors are designed based on instantaneous CSI to counteract channel fluctuations. More importantly, the antenna positions are optimized based on the long-term CSI, such as the signal power, the locations, the angles of arrival (AoAs), and the angles of departure (AoDs), which vary much slower than the instantaneous CSI. The antenna positions only need to be updated when there is a change in large-scale channel information. Unlike instantaneous CSI-based schemes, which require to update the antenna positions at each channel coherence interval, the two-timescale transmission design reduces both computational complexity and energy consumption, while effectively handling rapid channel variations and mitigating their impact. Nonetheless, the work in [32] only considered downlink transmission and assumed that perfect CSI is available. To deal with the difficulty of acquiring perfect CSI, [33] demonstrated a novel CSI-free fluid antenna position optimization method, which treats position optimization as a derivative-free problem, utilizing zeroth-order gradient approximation techniques to adaptively adjust the position. In the context of

imperfect CSI, the uplink two-timescale transmission scheme in MIMO-FAS remains an open issue.

To bridge this gap, this paper proposes a two-timescale uplink transmission scheme for a multiuser MIMO-FAS operating under a Rician fading channel with imperfect CSI. The optimization problem is inherently challenging due to the non-convexity of the objective function and constraints, as well as the requirement for expectation over random states. The main contributions of this work are summarized as follows:

- 1) First, we propose a two-timescale uplink transmission framework for multiuser MIMO-FAS that optimizes the antenna position based on statistical CSI, while optimizing BS's beamforming vectors based on instantaneous CSI. This hierarchical design significantly decreases fluid antenna reconfiguration frequency and channel estimation overhead.
- 2) Next, we consider the Rician channel model with imperfect CSI to assess the impact of the line-of-sight (LoS) and non-line-of-sight (NLoS) channel components. To estimate the channel at the BS, we employ the LMMSE method. Using a low-complexity maximal-ratio-combining (MRC) detector, we derive a closed-form expression for the use-and-then-forget (UatF) bound of the uplink achievable rate. This expression is valid for any finite number of fluid antennas and only depends on the statistical CSI.
- 3) We formulate an optimization problem to maximize the minimum user rate by optimizing the fluid antenna positions, subject to constraints on the feasible moving region for antennas and the minimum inter-antenna distance.
- 4) To solve this non-convex problem efficiently, we first propose a genetic algorithm (GA)-based method to obtain a suboptimal solution. In this approach, each individual in the population represents a specific realization of fluid antenna positions and its fitness function combines minimum user rate with a penalty term for constraint enforcement.
- 5) To further reduce the computational complexity, an accelerated gradient ascent-based algorithm is proposed to solve this fairness problem. This approach employs a log-sum-exp approximation to handle the non-differentiable minimum user rate maximization objective function, coupled with adaptive step size and projection operation to ensure antenna positions within the designated area.
- 6) Numerical results demonstrate that the proposed two-timescale framework for MIMO-FAS achieves significant improvement over the traditional FPA system with imperfect CSI. It is observed that both the GA-based method and the accelerated gradient ascent algorithm provide enhanced performance, offering a balance between accuracy and computational efficiency.

The remainder of this paper is structured as follows. Section II details the channel model and problem formulation. Section III analyzes the LMMSE channel estimation method. Section IV derives a closed-form lower bound expression of the

achievable rate. Section V proposes a GA-based method and an accelerated gradient ascent algorithm for solving the minimum user rate maximization optimization problem. Section VI illustrates numerical results, followed by conclusions in Section VII.

Notations: \mathcal{X} , \mathbf{X} , \mathbf{x} and x represent a set, a matrix, a vector, and a scalar, respectively. $(\cdot)^*$, $(\cdot)^T$, $(\cdot)^H$ and $(\cdot)^{-1}$ represent the conjugate, transpose, Hermitian transpose and inverse operation, respectively. $\mathbb{E}\{\cdot\}$ and $\text{Tr}\{\cdot\}$ denote the expectation and covariance operators. $[\mathbf{X}]_{m,n}$ denotes the (m, n) -th entry of the matrix. $\mathbb{R}^{M \times N}$ and $\mathbb{C}^{M \times N}$ are the space of $M \times N$ real and complex sets. $\mathbf{0}$ and \mathbf{I}_N are the $N \times N$ identity matrix and null vector. For the vector, $\|\cdot\|$ denotes the Euclidean norm and $|\cdot|$ denotes the modules of the complex number. $|\mathcal{X}|$ represents the cardinality of the set \mathcal{X} . $\mathbf{x} \sim \mathcal{CN}(\bar{\mathbf{x}}, \mathbf{C})$ represents a complex Gaussian distributed vector with mean vector $\bar{\mathbf{x}}$ and covariance matrix \mathbf{C} . $x \sim \mathcal{U}[m, n]$ indicates that x follows a uniform distribution within the range from m to n .

II. SYSTEM MODEL

A. Multiuser MIMO-FAS with imperfect CSI

As illustrated in Fig. 1, we consider an uplink transmission for multiuser MIMO-FAS, which consists of the BS equipped with M fluid antennas and the K users each equipped with a single transmit antenna. The positions of fluid antennas can be freely adjusted within a specified two-dimensional (2D) local region \mathcal{C} since they are connected to radio frequency chains via flexible cables, which allows the precise control of the system through electromechanical drivers such as stepper motors. Without loss of generality, let \mathcal{C} be a square region of size $A \times A$. The positions of all fluid antennas at the BS are represented as $\tilde{\mathbf{t}} = [\mathbf{t}_1, \mathbf{t}_2, \dots, \mathbf{t}_M] \in \mathbb{R}^{2 \times M}$, where $\mathbf{t}_m = [x_m, y_m]^T \in \mathcal{C}$ denotes the m -th fluid antenna position. The reference point of the region \mathcal{C} is $\mathbf{o} = [0, 0]^T$. For convenience, we denote the set of all fluid antennas as $\mathcal{M} = \{1, 2, \dots, M\}$, and the set of all users as $\mathcal{K} = \{1, 2, \dots, K\}$. The channel from the user $k, k \in \mathcal{K}$ to the BS is denoted by $\mathbf{h}_k \in \mathbb{C}^{M \times 1}$. Additionally, we define $\mathbf{H} = [\mathbf{h}_1, \mathbf{h}_2, \dots, \mathbf{h}_K]$. Therefore, the signal vector received at the BS can be written as

$$\mathbf{y} = \sqrt{p}\mathbf{H}\mathbf{x} + \mathbf{n} = \sqrt{p} \sum_{k=1}^K \mathbf{h}_k x_k + \mathbf{n}, \quad (1)$$

where p denotes the average transmit power of each user, $\mathbf{x} = [x_1, x_2, \dots, x_K]^T$ represents the information symbol vector of K users, and $\mathbf{n} \sim \mathcal{CN}(\mathbf{0}, \sigma^2 \mathbf{I}_M)$ is the additive white Gaussian noise (AWGN) with average power σ^2 .

We utilize a computationally efficient MRC technique to detect the information symbols at the BS. Before constructing the MRC matrix, the BS needs to estimate the channel \mathbf{H} . To this end, a conventional LMMSE estimator is applied, yielding the estimated channel $\hat{\mathbf{H}}$ based on some predefined pilot signals. We use τ_c to represent the length of the channel coherence interval, and τ to represent the number of time slots dedicated to channel estimation, where τ satisfies $\tau \geq K$. The details of the channel estimation will be elaborated in the next section. Based on the channel estimation, the BS performs

MRC detection by multiplying the received signal \mathbf{y} with $\hat{\mathbf{H}}^H$, which is given by

$$\mathbf{r} = \hat{\mathbf{H}}^H \mathbf{y} = \sqrt{p} \hat{\mathbf{H}}^H \mathbf{H} \mathbf{x} + \hat{\mathbf{H}}^H \mathbf{n}, \quad (2)$$

where \mathbf{r} represents the resulting signal after processing. Then, the k -th element of \mathbf{r} represents the detection signal for the k -th user, which can be further expressed as

$$\begin{aligned} r_k &= \sqrt{p} \hat{\mathbf{h}}_k^H \mathbf{h}_k x_k + \sqrt{p} \sum_{i=1, i \neq k}^K \hat{\mathbf{h}}_k^H \mathbf{h}_i x_i + \hat{\mathbf{h}}_k^H \mathbf{n} \\ &= \underbrace{\sqrt{p} \mathbb{E} \left\{ \hat{\mathbf{h}}_k^H \mathbf{h}_k \right\}}_{\text{Desired signal}} x_k + \underbrace{\sqrt{p} \left(\hat{\mathbf{h}}_k^H \mathbf{h}_k - \mathbb{E} \left\{ \hat{\mathbf{h}}_k^H \mathbf{h}_k \right\} \right)}_{\text{Signal leakage}} x_k \\ &\quad + \underbrace{\sqrt{p} \sum_{i=1, i \neq k}^K \hat{\mathbf{h}}_k^H \mathbf{h}_i x_i}_{\text{Multi-user interference}} + \underbrace{\hat{\mathbf{h}}_k^H \mathbf{n}}_{\text{Noise}}, \quad k \in \mathcal{K}, \end{aligned} \quad (3)$$

where $\hat{\mathbf{h}}_k$ denotes the k -th column of $\hat{\mathbf{H}}$.

B. Channel Model

We adopt the Rician fading model to describe the channel between user k and the BS, as follows

$$\begin{aligned} \mathbf{h}_k &= \sqrt{\frac{\alpha_k}{\varepsilon_k + 1}} \varepsilon_k \bar{\mathbf{h}}_k + \sqrt{\frac{\alpha_k}{\varepsilon_k + 1}} \tilde{\mathbf{h}}_k \\ &= \sqrt{c_k \varepsilon_k} \bar{\mathbf{h}}_k + \sqrt{c_k} \tilde{\mathbf{h}}_k, \end{aligned} \quad (4)$$

where α_k denotes the path-loss coefficient, ε_k denotes the Rician factor, $c_k \triangleq \frac{\alpha_k}{\varepsilon_k + 1}$ is auxiliary variable, $\bar{\mathbf{h}}_k \in \mathbb{C}^{M \times 1}$ represents the LoS component, and $\tilde{\mathbf{h}}_k \in \mathbb{C}^{M \times 1}$ represents the NLoS component. Specifically, for the NLoS path $\tilde{\mathbf{h}}_k$, the entries are independent and identically distributed (i.i.d) complex Gaussian random variables with zero mean and unit variance.

To better understand the LoS component $\bar{\mathbf{h}}_k$, we consider the characteristics of this system. It should be noted that this system works at a high frequency band, and the typical size of the antenna moving region is on the order of several to tens of wavelengths. Thus, we assume the size of the fluid antennas' movement region is significantly smaller than the signal propagation distance between the BS and the users, which makes the far-field condition easy to hold. In other words, for each channel path, AoDs, AoAs, and the amplitude of the complex channel coefficient are invariant, while only the phase of each path coefficient changes as a function of the fluid antenna positions.

Then, the difference in signal propagation distance for the LoS path between the m -th fluid antenna position \mathbf{t}_m and the reference position \mathbf{o} is given by

$$\begin{aligned} \rho_k^r(\mathbf{t}_m) &\triangleq \mathbf{t}_m^T [\sin \theta_{kr}^e \cos \theta_{kr}^a, \cos \theta_{kr}^e]^T \\ &= x_m \sin \theta_{kr}^e \cos \theta_{kr}^a + y_m \cos \theta_{kr}^e, \end{aligned} \quad (5)$$

where $\theta_{kr}^e \in [0, \pi]$ and $\theta_{kr}^a \in [0, \pi]$ are the elevation and azimuth AoAs of the incident signal at the BS from the user k , respectively. Accordingly, the resulting phase difference of the LoS path is $\frac{2\pi}{\lambda} \rho_k^r(\mathbf{t}_m)$, where λ denotes the carrier

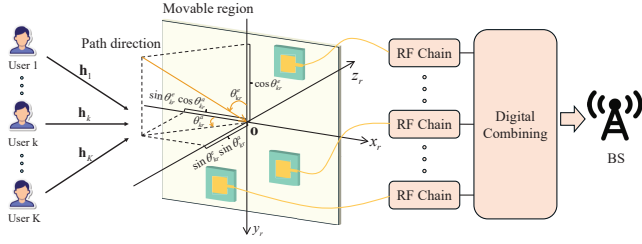


Fig. 1. System model: a multiuser MIMO-FAS

wavelength. Hence, for the LoS path, the channel vector $\bar{\mathbf{h}}_k(\mathbf{t})$ between the k -th user and the BS is given by

$$\bar{\mathbf{h}}_k(\tilde{\mathbf{t}}) = [e^{j\frac{2\pi}{\lambda}\rho_k^r(\mathbf{t}_1)}, e^{j\frac{2\pi}{\lambda}\rho_k^r(\mathbf{t}_2)}, \dots, e^{j\frac{2\pi}{\lambda}\rho_k^r(\mathbf{t}_M)}]^T. \quad (6)$$

C. Problem Formulation

For analytical tractability, we utilize the UatF bound [34], a practical lower bound, to characterize the capacity of the MIMO system. Thus, the lower bound of the k -th user's ergodic rate can be expressed as

$$\underline{R}_k(\tilde{\mathbf{t}}) = \frac{\tau_c - \tau}{\tau_c} \log_2(1 + \text{SINR}_k), \quad (7)$$

where the pre-log factor $\frac{\tau_c - \tau}{\tau_c}$ represents the rate loss due to the pilot overhead, and the SINR_k can be expressed as (8) at the top of the next page.

In this paper, we aim to maximize the minimum rate of all users through optimizing the matrix of fluid antenna positions $\tilde{\mathbf{t}}$ in the large timescale, thereby ensuring fairness among different users. The general optimization problem is then formulated as follows

$$\max_{\tilde{\mathbf{t}}} \min_{k \in \mathcal{K}} \underline{R}_k(\tilde{\mathbf{t}}), \quad (9a)$$

$$\text{s.t. } \|\mathbf{t}_m - \mathbf{t}_i\| \geq D_{\min}, \quad \forall m, i \in \mathcal{M}, m \neq i, \quad (9b)$$

$$\mathbf{t}_m \in \mathcal{C}, \quad \forall m \in \mathcal{M}, \quad (9c)$$

where constraint (9b) ensures the minimum spacing distance D_{\min} between any two adjacent fluid antennas to avoid coupling effects, and constraint (9c) indicates the feasible region of fluid antenna position. Notably, solving this max-min problem is highly challenging, because it involves not only a non-convex objective function (9a) and constraint (9c), but also the absence of a closed-form expression for the ergodic rate.

III. CHANNEL ESTIMATION

The BS estimates the CSI via the LMMSE method, utilizing received pilot signals occupying τ symbols within the channel coherence interval for uplink training. During the training process, all users simultaneously transmit mutually orthogonal pilot sequences, satisfying the orthogonality condition $\mathbf{S}^H \mathbf{S} = \mathbf{I}_K$ where $\mathbf{S} = [\mathbf{s}_1, \mathbf{s}_2, \dots, \mathbf{s}_K] \in \mathbb{C}^{\tau \times K}$ denotes the pilot matrix. Each transmitted pilot symbol carries power p , yielding total pilot power τp per user. Then, the $M \times \tau$ pilot signal matrix received at the BS is expressed as

$$\mathbf{Y}_p = \sqrt{\tau p} \mathbf{H} \mathbf{S}^H + \mathbf{N} = \sqrt{\tau p} \sum_{i=1}^K \mathbf{h}_i \mathbf{s}_i^H + \mathbf{N}, \quad (10)$$

where $\mathbf{N} \in \mathbb{C}^{M \times \tau}$ is a noise matrix with i.i.d $\mathcal{CN}(0, \sigma^2)$ elements. The observation signal for user k is obtained through multiplying (10) by $\frac{\mathbf{s}_k}{\sqrt{\tau p}}$, as follows

$$\mathbf{y}_p^k = \frac{1}{\sqrt{\tau p}} \mathbf{Y}_p \mathbf{s}_k = \mathbf{h}_k + \frac{\mathbf{N} \mathbf{s}_k}{\sqrt{\tau p}}. \quad (11)$$

Theorem 1 For $k \in \mathcal{K}$, the estimated channel vector $\hat{\mathbf{h}}_k$ obtained from the observation signal \mathbf{y}_p^k based on LMMSE estimator can be written as

$$\begin{aligned} \hat{\mathbf{h}}_k &= a_k \mathbf{y}_p^k + \mathbf{b}_k \\ &= \sqrt{c_k \varepsilon_k} \bar{\mathbf{h}}_k + a_k \sqrt{c_k} \tilde{\mathbf{h}}_k + \frac{a_k}{\sqrt{\tau p}} \mathbf{N} \mathbf{s}_k, \end{aligned} \quad (12)$$

$$a_k = \frac{c_k}{c_k + \frac{\sigma^2}{\tau p}}, \quad (13)$$

$$\mathbf{b}_k = (1 - a_k) \sqrt{c_k \varepsilon_k} \bar{\mathbf{h}}_k. \quad (14)$$

Proof: See Appendix A.

IV. ANALYSIS OF THE ACHIEVABLE RATE

In this section, the closed-form expression for a lower bound of the achievable rate is obtained by combining (7) with derived specific SINR_k expression, which exploits the estimated channel provided in Theorem 1 and the statistical CSI. The expression of SINR_k is given in the following theorem.

Theorem 2 The SINR for user k , $k \in \mathcal{K}$ in (7) is given by

$$\text{SINR}_k = \frac{p E_k^{\text{signal}}}{p E_k^{\text{leak}} + p \sum_{i=1, i \neq k}^K I_{ki} + \sigma^2 E_k^{\text{noise}}} \quad (15)$$

where

$$E_k^{\text{signal}} \triangleq \left| \mathbb{E} \left\{ \hat{\mathbf{h}}_k^H \mathbf{h}_k \right\} \right|^2, \quad (16)$$

$$E_k^{\text{leak}} \triangleq \mathbb{E} \left\{ \left| \hat{\mathbf{h}}_k^H \mathbf{h}_k \right|^2 \right\} - \left| \mathbb{E} \left\{ \hat{\mathbf{h}}_k^H \mathbf{h}_k \right\} \right|^2, \quad (17)$$

$$I_{ki} \triangleq \mathbb{E} \left\{ \left| \hat{\mathbf{h}}_k^H \mathbf{h}_i \right|^2 \right\}, \quad (18)$$

$$E_k^{\text{noise}} \triangleq \mathbb{E} \left\{ \left\| \hat{\mathbf{h}}_k \right\|^2 \right\}, \quad (19)$$

are respectively given in (20) - (23), shown at the top of the previous page, with

$$|f_k(\tilde{\mathbf{t}})|^2 = |\bar{\mathbf{h}}_k^H \bar{\mathbf{h}}_k|^2. \quad (24)$$

Proof: See Appendix B.

$$\text{SINR}_k = \frac{p \left| \mathbb{E} \left\{ \hat{\mathbf{h}}_k^H \mathbf{h}_k \right\} \right|^2}{p \left(\mathbb{E} \left\{ \left| \hat{\mathbf{h}}_k^H \mathbf{h}_k \right|^2 \right\} - \left| \mathbb{E} \left\{ \hat{\mathbf{h}}_k^H \mathbf{h}_k \right\} \right|^2 \right) + p \sum_{i=1, i \neq k}^K \mathbb{E} \left\{ \left| \hat{\mathbf{h}}_k^H \mathbf{h}_i \right|^2 \right\} + \sigma^2 \mathbb{E} \left\{ \left\| \hat{\mathbf{h}}_k \right\|^2 \right\}}. \quad (8)$$

$$E_k^{\text{signal}} = \{E_k^{\text{noise}}\}^2, \quad (20)$$

$$E_k^{\text{noise}} = M c_k (\varepsilon_k + a_k), \quad (21)$$

$$E_k^{\text{leak}} = M^2 c_k^2 \varepsilon_k^2 + M c_k^2 \varepsilon_k + M a_k^2 c_k^2 \varepsilon_k + a_k^2 c_k^2 M(M+1) + \frac{\sigma^2}{\tau p} M a_k^2 c_k \varepsilon_k + \frac{\sigma^2}{\tau p} a_k^2 c_k + 2M^2 c_k^2 a_k \varepsilon_k - M^2 c_k^2 (\varepsilon_k + a_k)^2, \quad (22)$$

$$I_{ki} = c_k c_i \varepsilon_k \varepsilon_i |f_k(\mathbf{t})|^2 + M c_k c_i \varepsilon_k + M a_k^2 c_k c_i \varepsilon_i + M a_k^2 c_k c_i + \frac{\sigma^2}{\tau p} M a_k^2 c_i \varepsilon_i + \frac{\sigma^2}{\tau p} a_k^2 c_i, \quad (23)$$

V. OPTIMIZATION OF THE ANTENNA POSITION

Optimizing the positions of fluid antennas presents significant challenges. On the one hand, the strong nonlinearity of $\underline{R}_k(\tilde{\mathbf{t}})$, coupled with the non-differentiable property of the max-min fairness objective, renders conventional optimization methods such as semidefinite relaxation (SDR) and majorization-minimization (MM) ineffective. On the other hand, the large solution space of the $\tilde{\mathbf{t}}$, i.e., $[-A/2, A/2]^{2M}$, makes exhaustive search methods prohibitive computational complexity. To address these challenges, we first propose a GA-based method. Although it is well-suited for the non-convex problem and search spaces, effectively avoiding local optima, the GA suffers from high computational complexity and slow convergence speed. Additionally, we propose an accelerated gradient ascent algorithm, which offers lower complexity and faster convergence when the objective function is differentiable, although it remains susceptible to local optima.

A. GA-based Solution

Rooted in biological evolutionary principles, GA emulates the evolution of a population in nature. In the GA-based approach, we first initialize N individuals forming the initial population $\mathcal{T}^{(0)} = \{\tilde{\mathbf{t}}_1^{(0)}, \tilde{\mathbf{t}}_2^{(0)}, \dots, \tilde{\mathbf{t}}_N^{(0)}\}$, where each individual represents potential antenna coordinates as follows

$$\tilde{\mathbf{t}}_n^{(0)} = [\mathbf{t}_{n,1}^{(0)}, \mathbf{t}_{n,2}^{(0)}, \dots, \mathbf{t}_{n,M}^{(0)}], \quad (25)$$

$$\mathbf{t}_{n,m}^{(0)} = [x_{n,m}^{(0)}, y_{n,m}^{(0)}]^T, \quad (26)$$

where $x_{n,m}^{(0)}, y_{n,m}^{(0)} \sim \mathcal{U}[-A/2, A/2]$ for $1 \leq n \leq N, 1 \leq m \leq M$ guarantee that the constraint (9c) holds. Additionally, to ensure that at least one individual has a positive fitness value, the position matrices of some individuals are initialized based on the uniform planar array (UPA) geometry with guaranteed minimum inter-antenna distance D_{\min} .

The fitness function incorporates adaptive penalty term to enforce constraint (9c), which is given by

$$\mathcal{F} \left\{ \tilde{\mathbf{t}}_n^{(i)} \right\} = \underline{R}_k \left(\tilde{\mathbf{t}}_n^{(i)} \right) - \omega \left| \mathcal{V} \left(\tilde{\mathbf{t}}_n^{(i)} \right) \right|, \quad (27)$$

where i denotes iteration index, ω is a large positive penalty parameter, and $\mathcal{V} \left(\tilde{\mathbf{t}}_n^{(i)} \right)$ is a defined set, whose elements

correspond to a pair positions of fluid antennas in $\tilde{\mathbf{t}}$ violating the minimum spacing distance D_{\min} , as follows

$$\begin{aligned} \mathcal{V}(\tilde{\mathbf{t}}) &= \{(\mathbf{t}_m, \mathbf{t}_{m'}) \mid \|\mathbf{t}_m - \mathbf{t}_{m'}\|_2 < D_{\min}, 1 \leq m < m' \leq M\}. \end{aligned} \quad (28)$$

The penalty parameter ω needs to ensure that $\underline{R}_k \left(\tilde{\mathbf{t}}_n^{(i)} \right) - \omega \leq 0$ holds for all individuals. If any individual violates the minimum spacing distance constraint, its fitness value will be less than zero. Therefore, in each iteration, all individuals can move toward positions that satisfy constraint (9b).

B. Low-complexity Gradient-based Solution

Although the GA-based method can simply solve this complicated problem, its computational complexity is relatively high. In this subsection, we adopt Nesterov's accelerated gradient ascent algorithm to solve this problem with lower complexity, achieving comparable performance. It is noted that this algorithm can effectively speed up the convergence rate of the gradient-based method to obtain better performance [35].

Due to the non-differentiable minimum function in the objective function (9a), the Lagrangian duality and the Jaynes maximum entropy principle are adopted. Then, an approximation of the minimum achievable user rate can be represented as follows

$$\min_{k \in \mathcal{K}} \underline{R}_k(\tilde{\mathbf{t}}) \approx -\frac{1}{\mu} \ln \left\{ \sum_{k=1}^K \exp\{-\mu \underline{R}_k(\tilde{\mathbf{t}})\} \right\} \triangleq g(\tilde{\mathbf{t}}), \quad (29)$$

where μ is a constant value that determines the approximation error to be less than $\frac{\ln K}{\mu}$, which has been proved in [36]. Thus, the problem can be recast as

$$\begin{aligned} &\max_{\tilde{\mathbf{t}}} g(\tilde{\mathbf{t}}), \\ &\text{s.t.} \quad (9b), (9c). \end{aligned} \quad (30)$$

Then, we need to calculate the gradient of $g(\tilde{\mathbf{t}})$. Based on the chain rule, we have

$$\frac{\partial g(\tilde{\mathbf{t}})}{\partial \tilde{\mathbf{t}}} = \frac{\tau_c - \tau}{\tau_c} \frac{\sum_{k=1}^K \left\{ \frac{\exp\{-\mu \underline{R}_k(\tilde{\mathbf{t}})\}}{1 + \text{SINR}_k(\tilde{\mathbf{t}})} \frac{\partial \text{SINR}_k(\tilde{\mathbf{t}})}{\partial \tilde{\mathbf{t}}} \right\}}{\ln 2 \left(\sum_{k=1}^K \exp\{-\mu \underline{R}_k(\tilde{\mathbf{t}})\} \right)}, \quad (31)$$

and

$$\frac{\partial \text{SINR}_k(\tilde{\mathbf{t}})}{\partial \tilde{\mathbf{t}}} = - \frac{p^2 E_k^{\text{signal}} \sum_{i=1, i \neq k}^K \frac{\partial I_{ki}(\tilde{\mathbf{t}})}{\partial \tilde{\mathbf{t}}}}{\left(p E_k^{\text{leak}} + p \sum_{i=1, i \neq k}^K I_{ki}(\tilde{\mathbf{t}}) + E_k^{\text{noise}} \right)^2}. \quad (32)$$

Thus, the gradient of $g(\tilde{\mathbf{t}})$ can be obtained after calculating $\frac{\partial I_{ki}(\tilde{\mathbf{t}})}{\partial \tilde{\mathbf{t}}}$.

Lemma 1 *The gradient of $I_{ki}(\tilde{\mathbf{t}})$ is given by*

$$\frac{\partial I_{ki}(\tilde{\mathbf{t}})}{\partial \tilde{\mathbf{t}}} = 2c_k c_i \epsilon_k \epsilon_i \text{Re} \left\{ \frac{\partial f_k(\tilde{\mathbf{t}})}{\partial \tilde{\mathbf{t}}} f_k^*(\tilde{\mathbf{t}}) \right\}, \quad (33)$$

$$\begin{aligned} & \left[\frac{\partial f_k(\tilde{\mathbf{t}})}{\partial \tilde{\mathbf{t}}} \right]_{1,u} \\ &= j \frac{2\pi}{\lambda} (\sin \theta_{ir}^e \cos \theta_{ir}^a - \sin \theta_{kr}^e \cos \theta_{kr}^a) e^{j \frac{2\pi}{\lambda} [\rho_i^r(\mathbf{t}_u) - \rho_k^r(\mathbf{t}_u)]}, \\ & \quad 1 \leq u \leq M, \end{aligned} \quad (34)$$

$$\begin{aligned} & \left[\frac{\partial f_k(\tilde{\mathbf{t}})}{\partial \tilde{\mathbf{t}}} \right]_{2,u} \\ &= j \frac{2\pi}{\lambda} (\cos \theta_{ir}^e - \cos \theta_{kr}^e) e^{j \frac{2\pi}{\lambda} [\rho_i^r(\mathbf{t}_u) - \rho_k^r(\mathbf{t}_u)]}, \\ & \quad 1 \leq u \leq M. \end{aligned} \quad (35)$$

Proof: First, we consider the gradient of $I_{ki}(\tilde{\mathbf{t}})$ through the chain rule.

$$\begin{aligned} \frac{\partial I_{ki}(\tilde{\mathbf{t}})}{\partial \tilde{\mathbf{t}}} &= c_k c_i \epsilon_k \epsilon_i \frac{\partial}{\partial \tilde{\mathbf{t}}} \left(|f_k(\tilde{\mathbf{t}})|^2 \right) \\ &= c_k c_i \epsilon_k \epsilon_i \frac{\partial}{\partial \tilde{\mathbf{t}}} \left(f_k(\tilde{\mathbf{t}}) f_k^*(\tilde{\mathbf{t}}) \right) \\ &= c_k c_i \epsilon_k \epsilon_i \left(\frac{\partial f_k(\tilde{\mathbf{t}})}{\partial \tilde{\mathbf{t}}} f_k^*(\tilde{\mathbf{t}}) + f_k(\tilde{\mathbf{t}}) \frac{\partial f_k^*(\tilde{\mathbf{t}})}{\partial \tilde{\mathbf{t}}} \right) \\ &= 2c_k c_i \epsilon_k \epsilon_i \text{Re} \left\{ \frac{\partial f_k(\tilde{\mathbf{t}})}{\partial \tilde{\mathbf{t}}} f_k^*(\tilde{\mathbf{t}}) \right\}, \end{aligned} \quad (36)$$

where $f_k^*(\tilde{\mathbf{t}})$ denotes the conjugate of $f_k(\tilde{\mathbf{t}})$. Therefore, (33) is proved.

Then, $\left[\frac{\partial f_k(\tilde{\mathbf{t}})}{\partial \tilde{\mathbf{t}}} \right]_{1,u}$, $\left[\frac{\partial f_k(\tilde{\mathbf{t}})}{\partial \tilde{\mathbf{t}}} \right]_{2,u}$, $1 \leq u \leq M$ represent the elements of the first row and the second row of the gradient matrix of $f_k(\tilde{\mathbf{t}})$, respectively, which are given by

$$\begin{aligned} \left[\frac{\partial f_k(\tilde{\mathbf{t}})}{\partial \tilde{\mathbf{t}}} \right]_{1,u} &= \left[\frac{\partial \bar{\mathbf{h}}_k^H(\tilde{\mathbf{t}}) \bar{\mathbf{h}}_i(\tilde{\mathbf{t}})}{\partial \tilde{\mathbf{t}}} \right]_{1,u} = \frac{\partial \bar{\mathbf{h}}_k^H(\tilde{\mathbf{t}}) \bar{\mathbf{h}}_i(\tilde{\mathbf{t}})}{\partial x_u} \\ &= \frac{\partial}{\partial x_u} \sum_{m=1}^M e^{j \frac{2\pi}{\lambda} [\rho_i^r(\mathbf{t}_m) - \rho_k^r(\mathbf{t}_m)]} \\ &= j \frac{2\pi}{\lambda} (\sin \theta_{ir}^e \cos \theta_{ir}^a - \sin \theta_{kr}^e \cos \theta_{kr}^a) e^{j \frac{2\pi}{\lambda} [\rho_i^r(\mathbf{t}_u) - \rho_k^r(\mathbf{t}_u)]}, \end{aligned} \quad (37)$$

$$\begin{aligned} \left[\frac{\partial f_k(\tilde{\mathbf{t}})}{\partial \tilde{\mathbf{t}}} \right]_{2,u} &= \left[\frac{\partial \bar{\mathbf{h}}_k^H(\tilde{\mathbf{t}}) \bar{\mathbf{h}}_i(\tilde{\mathbf{t}})}{\partial \tilde{\mathbf{t}}} \right]_{2,u} = \frac{\partial \bar{\mathbf{h}}_k^H(\tilde{\mathbf{t}}) \bar{\mathbf{h}}_i(\tilde{\mathbf{t}})}{\partial y_u} \\ &= \frac{\partial}{\partial y_u} \sum_{m=1}^M e^{j \frac{2\pi}{\lambda} [\rho_i^r(\mathbf{t}_m) - \rho_k^r(\mathbf{t}_m)]} \\ &= j \frac{2\pi}{\lambda} (\cos \theta_{ir}^e - \cos \theta_{kr}^e) e^{j \frac{2\pi}{\lambda} [\rho_i^r(\mathbf{t}_u) - \rho_k^r(\mathbf{t}_u)]}. \end{aligned} \quad (38)$$

Algorithm 1 Accelerated Gradient Ascent Algorithm

- 1: Initialize antenna positions $\tilde{\mathbf{t}}^{(0)}$ randomly and set $i = 0, l^{(0)} = 0.5, \mathbf{v}^{(-1)} = \tilde{\mathbf{t}}^{(0)}$;
 - 2: **while** 1 **do**
 - 3: Calculate the gradient matrix $\nabla_{\tilde{\mathbf{t}}} g(\tilde{\mathbf{t}}^{(i)})$;
 - 4: Obtain the step size $\zeta^{(i)}$ based on the backtracking line search until satisfying constraints (40a) and (40b);
 - 5: $\mathbf{v}^{(i)} = \mathcal{Y} \left\{ \tilde{\mathbf{t}}^{(i)} + \zeta^{(i)} \nabla_{\tilde{\mathbf{t}}} g(\tilde{\mathbf{t}}^{(i)}) \right\}$;
 - 6: $l^{(i+1)} = (1 + \sqrt{4l^{(i)^2 + 1})/2$;
 - 7: $\tilde{\mathbf{t}}^{(i+1)} = \mathcal{Y} \left\{ \mathbf{v}^{(i)} + (l^{(i)} - 1)(\mathbf{v}^{(i)} - \mathbf{v}^{(i-1)})/l^{(i+1)} \right\}$;
 - 8: **if** $g(\tilde{\mathbf{t}}^{(i+1)}) - g(\tilde{\mathbf{t}}^{(i)}) < 10^{-4}$ **then**
 - 9: $\tilde{\mathbf{t}}^* = \tilde{\mathbf{t}}^{(i+1)}$, **break**;
 - 10: **end if**
 - 11: $i = i + 1$;
 - 12: **end while**
-

Thus, (34) and (35) are established, which completes the proof.

By substituting (33), (34), and (35) into (31) and (32), the final analytical expression for the gradient of $g(\tilde{\mathbf{t}})$ can be obtained.

To guarantee the constraint in (9c), each update for the matrix of antenna positions is followed by a projection operation. Define $\mathcal{Y} \{ \tilde{\mathbf{t}} \}$ as projection function as follows

$$[\mathcal{Y}(\tilde{\mathbf{t}})]_{u,m} = \begin{cases} -\frac{A}{2}, & \text{if } [\tilde{\mathbf{t}}]_{u,m} < -\frac{A}{2}, \\ \frac{A}{2}, & \text{if } [\tilde{\mathbf{t}}]_{u,m} > \frac{A}{2}, \\ [\tilde{\mathbf{t}}]_{u,m}, & \text{otherwise,} \end{cases} \quad (39)$$

for $1 \leq u \leq 2, 1 \leq m \leq M$.

We assume the position matrix in the (i) -th iteration as $\tilde{\mathbf{t}}^{(i)}$, and the gradient of function $g(\tilde{\mathbf{t}}|\tilde{\mathbf{t}}^{(i)})$ at the antenna position matrix $\tilde{\mathbf{t}}^{(i)}$ in the (i) -th iteration as $\nabla_{\tilde{\mathbf{t}}} g(\tilde{\mathbf{t}}^{(i)}) = \frac{\partial g(\tilde{\mathbf{t}})}{\partial \tilde{\mathbf{t}}}|_{\tilde{\mathbf{t}}=\tilde{\mathbf{t}}^{(i)}}$. The convergence behavior of the gradient ascent method highly depends on the step length, which can be calculated based on the backtracking line search. To be specific, the initial step length is set a fixed value, and it iteratively decreases during the search process with a scaling factor $\kappa \in (0, 1)$, i.e., $\zeta^{(i)} \leftarrow \kappa \zeta^{(i-1)}$, until satisfies the Armijo-Goldstein condition and the minimum spacing constraint, as follows

$$g_{i-1}(\tilde{\mathbf{t}}^{(i)}) \geq g_{i-1}(\tilde{\mathbf{t}}^{(i-1)}) + \varpi \zeta^{(i)} \left\| \nabla_{\tilde{\mathbf{t}}} g_{i-1}(\tilde{\mathbf{t}}^{(i-1)}) \right\|^2, \quad (40a)$$

$$|\mathcal{P}(\tilde{\mathbf{t}}^{(i)})| = 0, \quad (40b)$$

where $\varpi \in (0, 1)$ denotes a control parameter to evaluate whether the step size is appropriate to enable the function $g(\tilde{\mathbf{t}}^{(i)})$ to increase efficiently. The main step of the low-complexity projected accelerated gradient ascent method is provided in Algorithm 1, where lines 6 and 7 correspond to the accelerated process.

VI. NUMERICAL RESULTS

In this section, numerical results of the multiuser MIMO-FAS with imperfect CSI are provided to validate the effectiveness of our two algorithms. We also analyze the impact

TABLE I
SIMULATION PARAMETERS

Parameter	Description	Value
λ	Carrier wavelength	0.1 m
A	Size of movable region	6λ
p	Transmit power	30 dBm
μ	Approximation factor	100
ω	Penalty factor	10
κ	Scaling factor	0.8
ϖ	Control parameter	0.5

of key parameters. The simulation considers a BS equipped with $M = 9$ fluid antennas serving $K = 3, 5, 7$ users, which are randomly distributed within $d_k \sim \mathcal{U}[50, 70]$ meters. The elevation and azimuth angles of AoDs and AoAs for each user and the BS are evenly distributed in the range of $[0, \lambda]$. Additionally, the movable region at the BS is set as $\mathcal{C} = [-A/2, A/2] \times [-A/2, A/2]$, and the minimum spacing between two adjacent fluid antennas is set as $D_{\min} = \frac{\lambda}{2}$. We set the large-scale path-loss coefficients equal to $\alpha_k = \alpha_0 d_k^{-2.8}, \forall k$, where $\alpha_0 = -40$ dB indicates the reference average path loss at 1 m. The Rician fading channel is modeled with a consistent Rician factor $\varepsilon_k = \varepsilon = 6, \forall k$, modeling moderate LoS condition. We assume that the length of the channel coherence interval as $\tau_c = 196$, and the number of symbols for channel estimation as $\tau = K$. The noise power is $\sigma^2 = -104$ dBm. Table I displays other simulation parameters and further specific parameters of the simulation are mentioned in the following.

Two proposed approaches are labeled by “**FAS-GA**” and “**FAS-gradient**”, which we compare with the following benchmark.

- **FPA**: The antennas at the BS are uniformly planar arrays with inter-element antenna spacing $\frac{\lambda}{2}$.

Fig. 2 illustrates the convergence behavior of the proposed FAS-GA scheme and the FAS-gradient scheme in a scenario with $M = 9$ fluid antennas at the BS and $K = 5$ users, and FAS-gradient scheme is further compared with the non-accelerated counterpart. As can be observed, the accelerated gradient approach converges within 100 times. Compared with the at least 250 iterations that use the non-accelerated gradient method, there is a significant enhancement in convergence speed. Additionally, although FAS-GA achieves convergence within 200 iterations, which has not much difference in the number of iterations with FAS-gradient, the total time consumption is reduced and the efficiency increases due to lower computational complexity in each iteration.

In Fig. 3, we explore the relationship between the number of users and achievable rate when $M = 7, 9$, accompanied by Monte Carlo simulation results. The Monte Carlo simulations are conducted to validate the correctness of mathematical derivations, which are obtained from (8) through averaging 10^5 random channel realizations, denoted as ‘Simulation’ in the figure legends. There is an excellent agreement between the approximate achievable rate expression in (7) and the

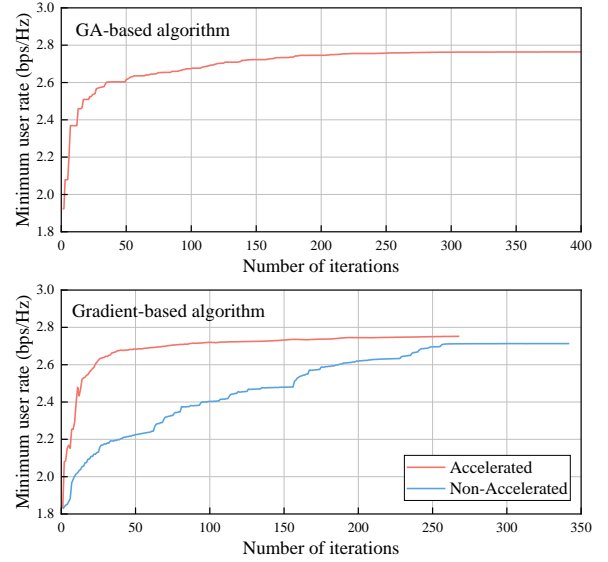


Fig. 2. Convergence performance of GA-based and Gradient-based algorithms.

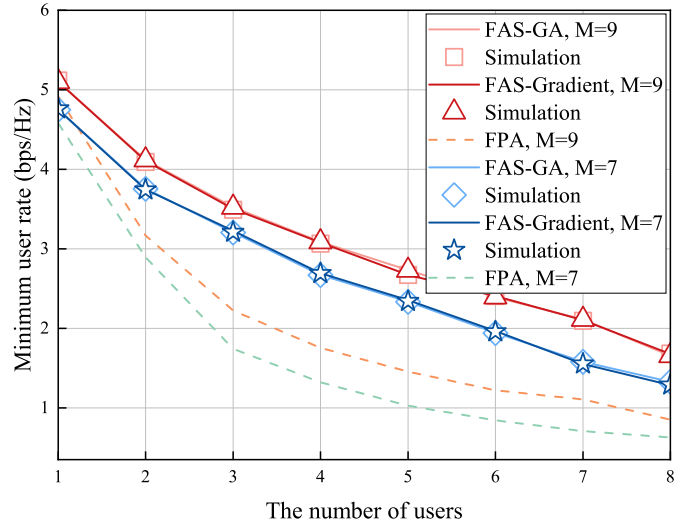


Fig. 3. Minimum user rate versus the number of users K .

simulation results. It is noted that FAS-GA and FAS-gradient provide nearly identical performance, delivering significant rate improvements over conventional FPA systems. Moreover, it can be observed that as the number of users K increases, the minimum user rate decreases, indicating that spatial diversity gains from fluid antennas cannot fully counteract intensified multiuser interference. Regardless of the number of users, the 9-antenna configuration consistently outperforms its 7-antenna counterpart.

For a clearer investigation into the number of fluid antennas, Fig. 4 shows the minimum user rate versus the number of fluid antennas for different user densities $K = 3, 5, 7$. There is an indistinguishable difference in performance between FAS-GA and FAS-gradient, with both consistently outperforming the FPA system. As shown in the figure, the minimum user rate exhibits monotonic growth with the number of fluid

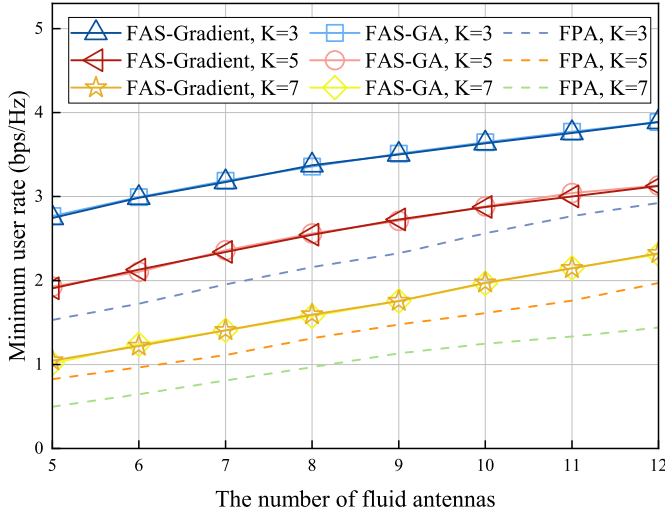


Fig. 4. Minimum user rate versus the number of antennas M .

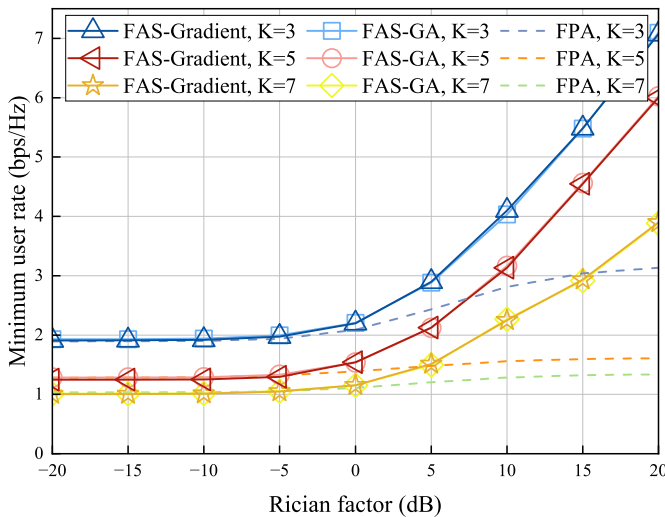


Fig. 5. Minimum user rate versus Rician factor ϵ .

antennas across all user configurations. This is attributed to enhanced spatial diversity gain enabled by additional antennas and interference suppression achieved through fluid antenna position optimization that impairs the multiuser interference term (23).

Fig. 5 reveals the influence of the Rician factor when the number of users is different. Across all cases, fluid antenna-enhanced schemes dramatically benefit from the increasing Rician factor ϵ . In weak LoS channel conditions where $\epsilon < -5$ dB, the minimum user rate for FAS-GA, FAS-gradient, and FPA schemes remains unchanged as ϵ increases, with the performance of three approaches nearly identical. As the channel becomes more predictable, the fluid antenna-assisted scheme demonstrates a greater optimization potential. When the Rician factor increases from 5 dB to 20 dB, the minimum user rate improves for various user scenarios, increasing from 1.9 bps/Hz to 7.1 bps/Hz for 3 users, from 1.2 bps/Hz to 6.0 bps/Hz for 5 users, and from 1.0 bps/Hz to 3.9 bps/Hz for 7 users.

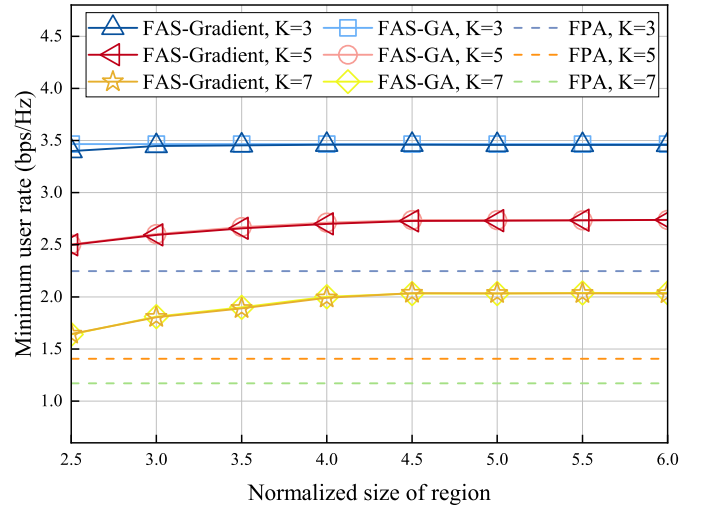


Fig. 6. Minimum user rate versus normalized size of region A/λ .

Finally, Fig. 6 displays the minimum user rate of three schemes for normalized movable region size A/λ . The performance of FAS-GA and FAS-gradient is closely matched. For $K = 7$, as the movable region increases, the minimum user rate of the fluid antenna-enhanced system rise from 1.64 bps/Hz to 2.03 bps/Hz at a diminishing speed, while that of the FPA approach is 1.17 bps/Hz, which indicates the position optimization achieves 73% performance improvement. For $K = 5$, the minimum user rate of the fluid antenna-enhanced system rise from 2.49 bps/Hz to 2.73 bps/Hz, while the FPA approach maintains a rate of 1.40 bps/Hz, resulting in a 95% performance gain. Notably, for $K = 3$, the minimum user rate remains approximately 3.46 bps/Hz within the Rician factor range of 2.5 to 6, which indicates it has converged. Compared to the FPA systems, FAS achieves a 54% improvement. These results indicate that expanding the feasible region allows the system to better exploit spatial DoFs, thereby enhancing spatial diversity and mitigating multiuser interference. However, as the movable region becomes sufficiently large, the FAS has fully utilized the spatial variations in the channel, leading to diminishing returns in performance improvement. Furthermore, for a lower number of users, the movable region required for convergence of the minimum user rate is smaller, suggesting that a more compact moving region is sufficient to achieve substantial performance gains with fewer users.

VII. CONCLUSION

This paper investigated the two-timescale uplink transmission design for multiuser MIMO-FAS with imperfect CSI. Specifically, the BS performed beamforming to adapt to fast-changing instantaneous CSI in the small timescale, while the fluid antenna positions were optimized based on statistical CSI in the large timescale. First, we applied the Rician channel model and estimated the channel at the BS utilizing the LMMSE estimator. The economical MRC detector was then used, and a closed-form expression of the achievable user rate was derived. The problem was formulated as the maximization of the minimum achievable rate for all users, subject to the

minimum spacing constraint and the feasible moving region constraint. Accordingly, a simple but computational complex GA-based method was proposed to tackle this non-convex problem. In order to reduce the complexity of numerical computation, an accelerated gradient ascent algorithm was introduced. Numerical results validated the potential of two algorithms for multiuser MIMO-FAS compared with traditional FPA schemes. Additionally, we examined the impact of key parameters on system performance.

APPENDIX A

Using the observation signal \mathbf{y}_p^k , the LMMSE estimate of the channel vector \mathbf{h}_k is given by [37]

$$\hat{\mathbf{h}}_k = \mathbb{E}\{\mathbf{h}_k\} + \text{Cov}\{\mathbf{h}_k, \mathbf{y}_p^k\} \text{Cov}^{-1}\{\mathbf{y}_p^k, \mathbf{y}_p^k\} (\mathbf{y}_p^k - \mathbb{E}\{\mathbf{y}_p^k\}). \quad (41)$$

The mean vectors and covariance matrices required in (41) for the channel vector \mathbf{h}_k and the observation signal \mathbf{y}_p^k are calculated step by step.

First, recalling the definition of \mathbf{y}_p^k , where $\tilde{\mathbf{h}}_k$ and \mathbf{N} are independent with zero-mean vector, the expectation term in (41) is given by

$$\mathbb{E}\{\mathbf{y}_p^k\} = \mathbb{E}\{\mathbf{h}_k\} + \frac{1}{\sqrt{\tau p}} \mathbb{E}\{\mathbf{N}\} \mathbf{s}_k = \mathbb{E}\{\mathbf{h}_k\}, \quad (42)$$

$$\mathbb{E}\{\mathbf{h}_k\} = \sqrt{c_k \varepsilon_k} \bar{\mathbf{h}}_k. \quad (43)$$

Then, the covariance matrices are given by

$$\begin{aligned} & \text{Cov}\{\mathbf{h}_k, \mathbf{h}_k\} \\ &= \mathbb{E}\left\{(\mathbf{h}_k - \mathbb{E}\{\mathbf{h}_k\})(\mathbf{h}_k - \mathbb{E}\{\mathbf{h}_k\})^H\right\} \\ &= c_k \mathbb{E}\left\{\tilde{\mathbf{h}}_k \tilde{\mathbf{h}}_k^H\right\} \\ &= c_k \mathbf{I}_M, \end{aligned} \quad (44)$$

$$\begin{aligned} & \text{Cov}\{\mathbf{h}_k, \mathbf{y}_p^k\} \\ &= \mathbb{E}\left\{(\mathbf{h}_k - \mathbb{E}\{\mathbf{h}_k\})(\mathbf{y}_p^k - \mathbb{E}\{\mathbf{y}_p^k\})^H\right\} \\ &= \mathbb{E}\left\{(\mathbf{h}_k - \mathbb{E}\{\mathbf{h}_k\})\left(\mathbf{h}_k + \frac{\mathbf{N}\mathbf{s}_k}{\sqrt{\tau p}} - \mathbb{E}\{\mathbf{h}_k\}\right)^H\right\} \\ &= \mathbb{E}\left\{(\mathbf{h}_k - \mathbb{E}\{\mathbf{h}_k\})(\mathbf{h}_k - \mathbb{E}\{\mathbf{h}_k\})^H\right. \\ &\quad \left. - (\mathbf{h}_k - \mathbb{E}\{\mathbf{h}_k\}) \frac{\mathbf{s}_k^H \mathbf{N}^H}{\sqrt{\tau p}}\right\} \\ &= \mathbb{E}\left\{(\mathbf{h}_k - \mathbb{E}\{\mathbf{h}_k\})(\mathbf{h}_k - \mathbb{E}\{\mathbf{h}_k\})^H\right\} \\ &= \text{Cov}\{\mathbf{h}_k, \mathbf{h}_k\}, \end{aligned} \quad (45)$$

$$\begin{aligned} & \text{Cov}\{\mathbf{y}_p^k, \mathbf{h}_k\} \\ &= (\text{Cov}\{\mathbf{h}_k, \mathbf{y}_p^k\})^H \\ &= \text{Cov}\{\mathbf{h}_k, \mathbf{h}_k\}, \end{aligned} \quad (46)$$

$$\begin{aligned} & \text{Cov}\{\mathbf{y}_p^k, \mathbf{y}_p^k\} \\ &= \mathbb{E}\left\{(\mathbf{y}_p^k - \mathbb{E}\{\mathbf{y}_p^k\})(\mathbf{y}_p^k - \mathbb{E}\{\mathbf{y}_p^k\})^H\right\} \\ &= \text{Cov}\{\mathbf{h}_k, \mathbf{h}_k\} + \frac{1}{\tau p} \mathbb{E}\{\mathbf{N}\mathbf{s}_k \mathbf{s}_k^H \mathbf{N}^H\} \\ &= \text{Cov}\{\mathbf{h}_k, \mathbf{h}_k\} + \frac{\sigma^2}{\tau p} \mathbf{I}_M \end{aligned}$$

$$= \left(c_k + \frac{\sigma^2}{\tau p}\right) \mathbf{I}_M. \quad (47)$$

Hence, the LMMSE channel estimate is calculated as

$$\begin{aligned} & \hat{\mathbf{h}}_k \\ &= \sqrt{c_k \varepsilon_k} \bar{\mathbf{h}}_k + c_k \left(c_k + \frac{\sigma^2}{\tau p}\right)^{-1} \mathbf{I}_M (\mathbf{y}_p^k - \sqrt{c_k \varepsilon_k} \bar{\mathbf{h}}_k) \\ &= \frac{c_k}{c_k + \frac{\sigma^2}{\tau p}} \mathbf{y}_p^k + \sqrt{c_k \varepsilon_k} \bar{\mathbf{h}}_k - \frac{c_k}{c_k + \frac{\sigma^2}{\tau p}} \sqrt{c_k \varepsilon_k} \bar{\mathbf{h}}_k \\ &= \frac{c_k}{c_k + \frac{\sigma^2}{\tau p}} \mathbf{y}_p^k + \frac{\frac{\sigma^2}{\tau p}}{c_k + \frac{\sigma^2}{\tau p}} \sqrt{c_k \varepsilon_k} \bar{\mathbf{h}}_k \\ &\triangleq a_k \mathbf{y}_k + \mathbf{b}_k \\ &= \frac{c_k}{c_k + \frac{\sigma^2}{\tau p}} \left(\mathbf{h}_k + \frac{1}{\tau p} \mathbf{N}\mathbf{s}_k\right) + \frac{\frac{\sigma^2}{\tau p}}{c_k + \frac{\sigma^2}{\tau p}} \sqrt{c_k \varepsilon_k} \bar{\mathbf{h}}_k \\ &= \frac{c_k}{c_k + \frac{\sigma^2}{\tau p}} \left(\sqrt{c_k \varepsilon_k} \bar{\mathbf{h}}_k + \sqrt{c_k} \tilde{\mathbf{h}}_k + \frac{1}{\tau p} \mathbf{N}\mathbf{s}_k\right) \\ &\quad + \frac{\frac{\sigma^2}{\tau p}}{c_k + \frac{\sigma^2}{\tau p}} \sqrt{c_k \varepsilon_k} \bar{\mathbf{h}}_k \\ &= \sqrt{c_k \varepsilon_k} \bar{\mathbf{h}}_k + \frac{c_k}{c_k + \frac{\sigma^2}{\tau p}} \sqrt{c_k} \tilde{\mathbf{h}}_k + \frac{c_k}{c_k + \frac{\sigma^2}{\tau p}} \frac{1}{\sqrt{\tau p}} \mathbf{N}\mathbf{s}_k \\ &= \sqrt{c_k \varepsilon_k} \bar{\mathbf{h}}_k + a_k \sqrt{c_k} \tilde{\mathbf{h}}_k + \frac{a_k}{\sqrt{\tau p}} \mathbf{N}\mathbf{s}_k. \end{aligned} \quad (48)$$

APPENDIX B

To begin with, we present some properties which will be useful in the following derivations.

Lemma 2 Let $\mathbf{X} \in \mathbb{C}^{m \times n}$, $m, n \geq 1$, be a matrix whose elements are i.i.d. random variables with zero mean and v_x variance. Consider a deterministic matrix $\mathbf{A} \in \mathbb{C}^{n \times n}$. Then, the following holds

$$\mathbb{E}\{\mathbf{X}\mathbf{A}\mathbf{X}^H\} = v_x \text{Tr}\{\mathbf{A}\} \mathbf{I}_m. \quad (49)$$

Proof: Consider the matrix $\mathbf{X}\mathbf{W}\mathbf{A}^H$. Due to the entries of \mathbf{X} are i.i.d with zero mean, the expectation of the (i, j) -th entry, where $i \neq j$, is given by

$$\begin{aligned} [\mathbb{E}\{\mathbf{X}\mathbf{A}\mathbf{X}^H\}]_{i,j} &= \mathbb{E}\left\{\sum_{l=1}^n \sum_{k=1}^n [\mathbf{X}]_{i,k} [\mathbf{A}]_{k,l} [\mathbf{X}^H]_{l,j}\right\} \\ &= \sum_{l=1}^n \sum_{k=1}^n \mathbb{E}\{[\mathbf{X}]_{i,k} [\mathbf{X}^*]_{j,l}\} [\mathbf{A}]_{k,l} = 0. \end{aligned} \quad (50)$$

Similarly, owing to the variance of \mathbf{X} elements, the expectation of the diagonal entry is

$$\begin{aligned} [\mathbb{E}\{\mathbf{X}\mathbf{A}\mathbf{X}^H\}]_{i,i} &= \sum_{l=1}^n \sum_{k=1}^n \mathbb{E}\{[\mathbf{X}]_{i,k} [\mathbf{X}^*]_{i,l}\} [\mathbf{A}]_{k,l} \\ &= \sum_{k=1}^n \mathbb{E}\{|[\mathbf{X}]_{i,k}|^2\} [\mathbf{A}]_{k,k} = v_x \text{Tr}\{\mathbf{A}\}. \end{aligned} \quad (51)$$

Thus, the expected value of $\mathbf{X}\mathbf{A}\mathbf{X}^H$ is a diagonal matrix, with each diagonal entry equal to $v_x \text{Tr}\{\mathbf{A}\}$. This completes the proof.

Lemma 3 Consider vectors $\mathbf{u}_1, \mathbf{u}_2 \in \mathbb{C}^{N \times 1}$, Then we have

$$\mathbb{E} \left\{ \mathbf{u}_1^H \tilde{\mathbf{h}}_k \mathbf{u}_2^H \tilde{\mathbf{h}}_k \right\} = \mathbb{E} \left\{ \text{Re} \left\{ \mathbf{u}_1^H \tilde{\mathbf{h}}_k \mathbf{u}_2^H \tilde{\mathbf{h}}_k \right\} \right\} = 0, \quad (52)$$

$$\mathbb{E} \left\{ \left\| \tilde{\mathbf{h}}_k \right\|^4 \right\} = \text{Tr} \left\{ \mathbb{E} \left\{ \tilde{\mathbf{h}}_k \tilde{\mathbf{h}}_k^H \tilde{\mathbf{h}}_k \tilde{\mathbf{h}}_k^H \right\} \right\} = M^2 + M. \quad (53)$$

Proof: Let $v = v_r + jv_i$ represents a complex random variable, where v_r and v_i are independent and normally distributed with zero mean and variance $\frac{1}{2}$, i.e., $v_r, v_i \sim \mathcal{N}(0, \frac{1}{2})$. From this, we derive

$$\mathbb{E} \{v^2\} = \mathbb{E} \{v_r^2 - v_i^2 + 2jv_r v_i\} = 0, \quad (54)$$

$$\mathbb{E} \{\text{Re}\{v^2\}\} = \mathbb{E} \{v_r^2\} - \mathbb{E} \{v_i^2\} = 0. \quad (55)$$

The entries of $\tilde{\mathbf{h}}_k$ are i.i.d, each following the same distribution as v . Then, we can express the expectation of (52) as

$$\begin{aligned} & \mathbb{E} \left\{ \mathbf{u}_1^H \tilde{\mathbf{h}}_k \mathbf{u}_2^H \tilde{\mathbf{h}}_k \right\} \\ &= \mathbb{E} \left\{ \sum_{n_1=1}^M \sum_{n_2=1}^M [\mathbf{u}_1^H]_{n_1} [\mathbf{u}_2^H]_{n_2} [\tilde{\mathbf{h}}_k]_{n_1} [\tilde{\mathbf{h}}_k]_{n_2} \right\}. \end{aligned} \quad (56)$$

When $n_1 \neq n_2$, the expectation $\mathbb{E} \left\{ [\mathbf{u}_1^H]_{n_1} [\mathbf{u}_2^H]_{n_2} [\tilde{\mathbf{h}}_k]_{n_1} [\tilde{\mathbf{h}}_k]_{n_2} \right\}$ vanishes due to the independence and zero mean of the elements of $\tilde{\mathbf{h}}_k$. When $n_1 = n_2$, the expectation becomes zero according to (54). Hence, (52) is verified.

Next, consider the expectation of $\left\| \tilde{\mathbf{h}}_k \right\|^4$, which can be expressed as

$$\begin{aligned} \mathbb{E} \left\{ \left\| \tilde{\mathbf{h}}_k \right\|^4 \right\} &= \mathbb{E} \left\{ \left(\sum_{i=1}^M \left| [\tilde{\mathbf{h}}_k]_i \right|^2 \right)^2 \right\} \\ &= \mathbb{E} \left\{ \sum_{i=1}^M \left| [\tilde{\mathbf{h}}_k]_i \right|^4 \right\} + \mathbb{E} \left\{ \sum_{i \neq j} \left| [\tilde{\mathbf{h}}_k]_i \right|^2 \left| [\tilde{\mathbf{h}}_k]_j \right|^2 \right\} \\ &= 2M + M(M-1) = M^2 + M. \end{aligned} \quad (57)$$

Therefore, (53) is established, completing the proof.

A. Signal Term and Noise Term

Based on the estimated channel $\hat{\mathbf{h}}_k$ in (12), the estimation error $\mathbf{e}_k = \mathbf{h}_k - \hat{\mathbf{h}}_k$ has zero mean. Then, according to the orthogonality of the LMMSE estimator, we can obtain $\mathbb{E} \left\{ \mathbf{e}_k (\mathbf{y}_p^k)^H \right\} = \mathbf{0}$, and it follows that $\mathbb{E} \left\{ \hat{\mathbf{h}}_k^H \mathbf{e}_k \right\} = \mathbf{0}$. Therefore, We have

$$\mathbb{E} \left\{ \hat{\mathbf{h}}_k^H \mathbf{h}_k \right\} = \mathbb{E} \left\{ \hat{\mathbf{h}}_k^H \hat{\mathbf{h}}_k \right\} + \mathbb{E} \left\{ \hat{\mathbf{h}}_k^H \mathbf{e}_k \right\} = \mathbb{E} \left\{ \left\| \hat{\mathbf{h}}_k \right\|^2 \right\}. \quad (58)$$

Hence, the signal power can be expressed as

$$E_k^{\text{signal}} = \left| \mathbb{E} \left\{ \hat{\mathbf{h}}_k^H \mathbf{h}_k \right\} \right|^2 = \left(\mathbb{E} \left\{ \left\| \hat{\mathbf{h}}_k \right\|^2 \right\} \right)^2 = (E_k^{\text{noise}})^2. \quad (59)$$

Then, the noise term can be expanded as

$$\begin{aligned} E_k^{\text{noise}} &= \mathbb{E} \left\{ \left\| \hat{\mathbf{h}}_k \right\|^2 \right\} = \mathbb{E} \left\{ \hat{\mathbf{h}}_k^H \mathbf{h}_k \right\} \\ &= \mathbb{E} \left\{ \left(\sqrt{c_k \varepsilon_k} \bar{\mathbf{h}}_k + a_k \sqrt{c_k} \tilde{\mathbf{h}}_k + \frac{a_k}{\sqrt{\tau p}} \mathbf{N} \mathbf{s}_k \right)^H \right. \\ &\quad \left. \left(\sqrt{c_k \varepsilon_k} \bar{\mathbf{h}}_k + \sqrt{c_k} \tilde{\mathbf{h}}_k \right) \right\} \\ &= c_k \varepsilon_k \bar{\mathbf{h}}_k^H \bar{\mathbf{h}}_k + a_k c_k \mathbb{E} \left\{ \tilde{\mathbf{h}}_k^H \tilde{\mathbf{h}}_k \right\} \\ &= M c_k (\varepsilon_k + a_k). \end{aligned} \quad (60)$$

B. Signal Leakage

The signal leakage can be expressed as $E_k^{\text{leak}} = \mathbb{E} \left\{ \left| \hat{\mathbf{h}}_k^H \mathbf{h}_k \right|^2 \right\} - \left| \mathbb{E} \left\{ \hat{\mathbf{h}}_k^H \mathbf{h}_k \right\} \right|^2$ in (17), where $\mathbb{E} \left\{ \hat{\mathbf{h}}_k^H \mathbf{h}_k \right\}$ is given in (60), and $\mathbb{E} \left\{ \left| \hat{\mathbf{h}}_k^H \mathbf{h}_k \right|^2 \right\}$ will be derived by exploiting the independence between the channel and the noise, as follows

$$\begin{aligned} & \mathbb{E} \left\{ \left| \hat{\mathbf{h}}_k^H \mathbf{h}_k \right|^2 \right\} \\ &= \mathbb{E} \left\{ \left| \left(\sqrt{c_k \varepsilon_k} \bar{\mathbf{h}}_k + a_k \sqrt{c_k} \tilde{\mathbf{h}}_k + \frac{a_k}{\sqrt{\tau p}} \mathbf{N} \mathbf{s}_k \right)^H \right. \right. \\ &\quad \left. \left. \left(\sqrt{c_k \varepsilon_k} \bar{\mathbf{h}}_k + \sqrt{c_k} \tilde{\mathbf{h}}_k \right) \right|^2 \right\} \\ &= \mathbb{E} \left\{ \left| c_k \varepsilon_k \bar{\mathbf{h}}_k^H \bar{\mathbf{h}}_k + c_k \sqrt{\varepsilon_k} \bar{\mathbf{h}}_k^H \tilde{\mathbf{h}}_k \right. \right. \\ &\quad \left. \left. + a_k c_k \sqrt{\varepsilon_k} \tilde{\mathbf{h}}_k^H \bar{\mathbf{h}}_k + a_k c_k \tilde{\mathbf{h}}_k^H \tilde{\mathbf{h}}_k \right. \right. \\ &\quad \left. \left. + \frac{a_k}{\sqrt{\tau p}} \sqrt{c_k \varepsilon_k} \mathbf{s}_k^H \mathbf{N}^H \bar{\mathbf{h}}_k + \frac{a_k}{\sqrt{\tau p}} \sqrt{c_k} \mathbf{s}_k^H \mathbf{N}^H \tilde{\mathbf{h}}_k \right|^2 \right\} \\ &= \left| c_k \varepsilon_k \bar{\mathbf{h}}_k^H \bar{\mathbf{h}}_k \right|^2 + \mathbb{E} \left\{ \left| c_k \sqrt{\varepsilon_k} \bar{\mathbf{h}}_k^H \tilde{\mathbf{h}}_k \right|^2 \right\} \\ &\quad + \mathbb{E} \left\{ \left| a_k c_k \sqrt{\varepsilon_k} \tilde{\mathbf{h}}_k^H \bar{\mathbf{h}}_k \right|^2 \right\} + \mathbb{E} \left\{ \left| a_k c_k \tilde{\mathbf{h}}_k^H \tilde{\mathbf{h}}_k \right|^2 \right\} \\ &\quad + \mathbb{E} \left\{ \left| \frac{a_k}{\sqrt{\tau p}} \sqrt{c_k \varepsilon_k} \mathbf{s}_k^H \mathbf{N}^H \bar{\mathbf{h}}_k \right|^2 \right\} \\ &\quad + \mathbb{E} \left\{ \left| \frac{a_k}{\sqrt{\tau p}} \sqrt{c_k} \mathbf{s}_k^H \mathbf{N}^H \tilde{\mathbf{h}}_k \right|^2 \right\} \\ &\quad + 2 \text{Re} \left\{ \mathbb{E} \left\{ c_k^2 a_k \varepsilon_k \bar{\mathbf{h}}_k^H \bar{\mathbf{h}}_k \tilde{\mathbf{h}}_k^H \tilde{\mathbf{h}}_k \right\} \right\}. \end{aligned} \quad (61)$$

Then, the seven terms in (61) will be calculated as follows

$$\left| c_k \varepsilon_k \bar{\mathbf{h}}_k^H \bar{\mathbf{h}}_k \right|^2 = M^2 c_k^2 \varepsilon_k^2, \quad (62)$$

$$\mathbb{E} \left\{ \left| c_k \sqrt{\varepsilon_k} \bar{\mathbf{h}}_k^H \tilde{\mathbf{h}}_k \right|^2 \right\} = c_k^2 \varepsilon_k \bar{\mathbf{h}}_k^H \mathbb{E} \left\{ \tilde{\mathbf{h}}_k \tilde{\mathbf{h}}_k^H \right\} \bar{\mathbf{h}}_k = M c_k^2 \varepsilon_k, \quad (63)$$

$$\begin{aligned} \mathbb{E} \left\{ \left| a_k c_k \sqrt{\varepsilon_k} \tilde{\mathbf{h}}_k^H \bar{\mathbf{h}}_k \right|^2 \right\} &= a_k^2 c_k^2 \varepsilon_k \mathbb{E} \left\{ \tilde{\mathbf{h}}_k^H \bar{\mathbf{h}}_k \bar{\mathbf{h}}_k^H \tilde{\mathbf{h}}_k \right\} \\ &\stackrel{(a)}{=} a_k^2 c_k^2 \varepsilon_k \text{Tr} \left\{ \bar{\mathbf{h}}_k \bar{\mathbf{h}}_k^H \right\} = M a_k^2 c_k^2 \varepsilon_k, \end{aligned} \quad (64)$$

$$\begin{aligned} & \mathbb{E} \left\{ \left| a_k c_k \tilde{\mathbf{h}}_k^H \tilde{\mathbf{h}}_k \right|^2 \right\} \\ &= a_k^2 c_k^2 \mathbb{E} \left\{ \tilde{\mathbf{h}}_k^H \tilde{\mathbf{h}}_k \tilde{\mathbf{h}}_k^H \tilde{\mathbf{h}}_k \right\} \stackrel{(b)}{=} M(M+1) a_k^2 c_k^2, \end{aligned} \quad (65)$$

$$\begin{aligned}
& \mathbb{E} \left\{ \left| \frac{a_k}{\sqrt{\tau p}} \sqrt{c_k \varepsilon_k} \mathbf{s}_k^H \mathbf{N}^H \bar{\mathbf{h}}_k \right|^2 \right\} \\
&= \frac{1}{\tau p} a_k^2 c_k \varepsilon_k \mathbb{E} \left\{ \mathbf{s}_k^H \mathbf{N}^H \bar{\mathbf{h}}_k \bar{\mathbf{h}}_k^H \mathbf{N} \mathbf{s}_k \right\} \\
&= \frac{1}{\tau p} a_k^2 c_k \varepsilon_k \mathbf{s}_k^H \mathbb{E} \left\{ \mathbf{N}^H \bar{\mathbf{h}}_k \bar{\mathbf{h}}_k^H \mathbf{N} \right\} \mathbf{s}_k \\
&\stackrel{(c)}{=} \frac{\sigma^2}{\tau p} a_k^2 c_k \varepsilon_k \mathbf{s}_k^H \text{Tr} \left\{ \bar{\mathbf{h}}_k \bar{\mathbf{h}}_k^H \right\} \mathbf{s}_k \\
&= \frac{\sigma^2}{\tau p} M a_k^2 c_k \varepsilon_k,
\end{aligned} \tag{66}$$

$$\begin{aligned}
& \mathbb{E} \left\{ \left| \frac{a_k}{\sqrt{\tau p}} \sqrt{c_k} \mathbf{s}_k^H \mathbf{N}^H \tilde{\mathbf{h}}_k \right|^2 \right\} \\
&= \frac{1}{\tau p} a_k^2 c_k \mathbb{E} \left\{ \mathbf{s}_k^H \mathbf{N}^H \tilde{\mathbf{h}}_k \tilde{\mathbf{h}}_k^H \mathbf{N} \mathbf{s}_k \right\} \\
&= \frac{1}{\tau p} a_k^2 c_k \mathbf{s}_k^H \mathbb{E} \left\{ \mathbf{N}^H \mathbb{E} \left\{ \tilde{\mathbf{h}}_k \tilde{\mathbf{h}}_k^H \right\} \mathbf{N} \right\} \mathbf{s}_k \\
&= \frac{\sigma^2}{\tau p} a_k^2 c_k,
\end{aligned} \tag{67}$$

$$\begin{aligned}
& 2\text{Re} \left\{ \mathbb{E} \left\{ c_k^2 a_k \varepsilon_k \bar{\mathbf{h}}_k^H \bar{\mathbf{h}}_k \tilde{\mathbf{h}}_k^H \tilde{\mathbf{h}}_k \right\} \right\} \\
&= 2c_k^2 a_k \varepsilon_k \text{Re} \left\{ \bar{\mathbf{h}}_k^H \bar{\mathbf{h}}_k \mathbb{E} \left\{ \tilde{\mathbf{h}}_k^H \tilde{\mathbf{h}}_k \right\} \right\} \\
&= 2M^2 c_k^2 a_k \varepsilon_k,
\end{aligned} \tag{68}$$

where (a) and (c) apply Lemma 2, and (b) applies Lemma 3. Thus, we can obtain the $\mathbb{E} \left\{ \left| \hat{\mathbf{h}}_k^H \mathbf{h}_k \right|^2 \right\}$ by combining (62)-(68) with (61). With the aid of (60), we can complete the calculation of the signal leakage term E_k^{leak} using (17).

C. Interference Term

To begin, we obtain the interference term by breaking it down as follows

$$\begin{aligned}
I_{ki} &\triangleq \mathbb{E} \left\{ \left| \hat{\mathbf{h}}_k^H \mathbf{h}_i \right|^2 \right\} \\
&= \mathbb{E} \left\{ \left| \left(\sqrt{c_k \varepsilon_k} \bar{\mathbf{h}}_k + a_k \sqrt{c_k} \tilde{\mathbf{h}}_k + \frac{a_k}{\sqrt{\tau p}} \mathbf{N} \mathbf{s}_k \right)^H \right. \right. \\
&\quad \left. \left. \left(\sqrt{c_i \varepsilon_i} \bar{\mathbf{h}}_i + \sqrt{c_i} \tilde{\mathbf{h}}_i \right) \right|^2 \right\} \\
&= \mathbb{E} \left\{ \left| \sqrt{c_k c_i \varepsilon_k \varepsilon_i} \bar{\mathbf{h}}_k^H \bar{\mathbf{h}}_i + \sqrt{c_k c_i \varepsilon_k} \bar{\mathbf{h}}_k^H \tilde{\mathbf{h}}_i \right. \right. \\
&\quad \left. \left. + a_k \sqrt{c_k c_i \varepsilon_i} \tilde{\mathbf{h}}_k^H \bar{\mathbf{h}}_i + a_k \sqrt{c_k c_i} \tilde{\mathbf{h}}_k^H \tilde{\mathbf{h}}_i \right. \right. \\
&\quad \left. \left. + \frac{a_k}{\sqrt{\tau p}} \sqrt{c_i \varepsilon_i} \mathbf{s}_k^H \mathbf{N}^H \bar{\mathbf{h}}_i + \frac{a_k}{\sqrt{\tau p}} \sqrt{c_i} \mathbf{s}_k^H \mathbf{N}^H \tilde{\mathbf{h}}_i \right|^2 \right\} \\
&= \left| \sqrt{c_k c_i \varepsilon_k \varepsilon_i} \bar{\mathbf{h}}_k^H \bar{\mathbf{h}}_i \right|^2 + \mathbb{E} \left\{ \left| \sqrt{c_k c_i \varepsilon_k} \bar{\mathbf{h}}_k^H \tilde{\mathbf{h}}_i \right|^2 \right\} \\
&\quad + \mathbb{E} \left\{ \left| a_k \sqrt{c_k c_i \varepsilon_i} \tilde{\mathbf{h}}_k^H \bar{\mathbf{h}}_i \right|^2 \right\} + \mathbb{E} \left\{ \left| a_k \sqrt{c_k c_i} \tilde{\mathbf{h}}_k^H \tilde{\mathbf{h}}_i \right|^2 \right\} \\
&\quad + \mathbb{E} \left\{ \left| \frac{a_k}{\sqrt{\tau p}} \sqrt{c_i \varepsilon_i} \mathbf{s}_k^H \mathbf{N}^H \bar{\mathbf{h}}_i \right|^2 \right\} \\
&\quad + \mathbb{E} \left\{ \left| \frac{a_k}{\sqrt{\tau p}} \sqrt{c_i} \mathbf{s}_k^H \mathbf{N}^H \tilde{\mathbf{h}}_i \right|^2 \right\}.
\end{aligned} \tag{69}$$

Then, the six term in (69) will be given by

$$\left| \sqrt{c_k c_i \varepsilon_k \varepsilon_i} \bar{\mathbf{h}}_k^H \bar{\mathbf{h}}_i \right|^2 = c_k c_i \varepsilon_k \varepsilon_i \left| \bar{\mathbf{h}}_k^H \bar{\mathbf{h}}_i \right|^2 = c_k c_i \varepsilon_k \varepsilon_i \left| f_k(\tilde{\mathbf{t}}) \right|^2, \tag{70}$$

$$\begin{aligned}
& \mathbb{E} \left\{ \left| \sqrt{c_k c_i \varepsilon_k} \bar{\mathbf{h}}_k^H \tilde{\mathbf{h}}_i \right|^2 \right\} = c_k c_i \varepsilon_k \bar{\mathbf{h}}_k^H \mathbb{E} \left\{ \tilde{\mathbf{h}}_i \tilde{\mathbf{h}}_i^H \right\} \bar{\mathbf{h}}_k \\
&= M c_k c_i \varepsilon_k,
\end{aligned} \tag{71}$$

$$\begin{aligned}
& \mathbb{E} \left\{ \left| a_k \sqrt{c_k c_i \varepsilon_i} \tilde{\mathbf{h}}_k^H \bar{\mathbf{h}}_i \right|^2 \right\} = a_k^2 c_k c_i \varepsilon_i \mathbb{E} \left\{ \tilde{\mathbf{h}}_k^H \bar{\mathbf{h}}_i \bar{\mathbf{h}}_i^H \tilde{\mathbf{h}}_k \right\} \\
&\stackrel{(d)}{=} a_k^2 c_k c_i \varepsilon_i \text{Tr} \left\{ \bar{\mathbf{h}}_i \bar{\mathbf{h}}_i^H \right\} = M a_k^2 c_k c_i \varepsilon_i,
\end{aligned} \tag{72}$$

$$\begin{aligned}
& \mathbb{E} \left\{ \left| a_k \sqrt{c_k c_i} \tilde{\mathbf{h}}_k^H \tilde{\mathbf{h}}_i \right|^2 \right\} \\
&= a_k^2 c_k c_i \mathbb{E} \left\{ \tilde{\mathbf{h}}_k^H \mathbb{E} \left\{ \tilde{\mathbf{h}}_i \tilde{\mathbf{h}}_i^H \right\} \tilde{\mathbf{h}}_k \right\} = M a_k^2 c_k c_i,
\end{aligned} \tag{73}$$

$$\begin{aligned}
& \mathbb{E} \left\{ \left| \frac{a_k}{\tau p} \sqrt{c_i \varepsilon_i} \mathbf{s}_k^H \mathbf{N}^H \bar{\mathbf{h}}_i \right|^2 \right\} \\
&= \frac{1}{\tau p} a_k^2 c_i \varepsilon_i \mathbf{s}_k^H \mathbb{E} \left\{ \mathbf{N}^H \bar{\mathbf{h}}_i \bar{\mathbf{h}}_i^H \mathbf{N} \right\} \mathbf{s}_k \\
&\stackrel{(e)}{=} \frac{\sigma^2}{\tau p} a_k^2 c_i \varepsilon_i \mathbf{s}_k^H \text{Tr} \left\{ \bar{\mathbf{h}}_i \bar{\mathbf{h}}_i^H \right\} \mathbf{s}_k \\
&= \frac{\sigma^2}{\tau p} M a_k^2 c_i \varepsilon_i,
\end{aligned} \tag{74}$$

$$\begin{aligned}
& \mathbb{E} \left\{ \left| \frac{a_k}{\tau p} \sqrt{c_i} \mathbf{s}_k^H \mathbf{N}^H \tilde{\mathbf{h}}_i \right|^2 \right\} \\
&= \frac{1}{\tau p} a_k^2 c_i \mathbf{s}_k^H \mathbb{E} \left\{ \mathbf{N}^H \mathbb{E} \left\{ \tilde{\mathbf{h}}_i \tilde{\mathbf{h}}_i^H \right\} \mathbf{N} \right\} \mathbf{s}_k = \frac{\sigma^2}{\tau p} a_k^2 c_i,
\end{aligned} \tag{75}$$

where (d) and (e) apply Lemma 2. Consequently, the calculation is finalized, and the interference term is obtained by integrating (70) - (75) with (69).

REFERENCES

- [1] A. Fayad, T. Cinkler, and J. Rak, "Toward 6G optical fronthaul: A survey on enabling technologies and research perspectives," *IEEE Commun. Surv. Tutorials*, vol. 27, no. 1, pp. 629–666, Feb. 2024.
- [2] L. Zheng and D. N. C. Tse, "Diversity and multiplexing: A fundamental tradeoff in multiple-antenna channels," *IEEE Trans. Inf. Theory*, vol. 49, no. 5, pp. 1073–1096, May 2003.
- [3] X. Shao, Q. Jiang, and R. Zhang, "6D movable antenna based on user distribution: Modeling and optimization," *IEEE Trans. Wireless Commun.*, vol. 24, no. 1, pp. 355–370, Jan. 2025.
- [4] E. G. Larsson, O. Edfors, F. Tufvesson, and T. L. Marzetta, "Massive MIMO for next generation wireless systems," *IEEE Commun. Mag.*, vol. 52, no. 2, pp. 186–195, Feb. 2014.
- [5] L. Jing, M. Li, and R. Murch, "Compact pattern reconfigurable pixel antenna with diagonal pixel connections," *IEEE Trans. Antennas Propag.*, vol. 70, no. 10, pp. 8951–8961, Oct. 2022.
- [6] S. Dash, C. Psomas, and I. Krikididis, "Selection of metallic liquid in sub-6 GHz antenna design for 6G networks," *Sci. Rep.*, vol. 13, no. 1, p. 20551, Nov. 2023.
- [7] S. Basbug, "Design and synthesis of antenna array with movable elements along semicircular paths," *IEEE Antennas Wirel. Propag. Lett.*, vol. 16, pp. 3059–3062, 2017.
- [8] K.-K. Wong, K.-F. Tong, Y. Shen, Y. Chen, and Y. Zhang, "Bruce lea-inspired fluid antenna system: Six research topics and the potentials for 6G," *Front. commun. netw.*, vol. 3, p. 853416, Mar. 2022.
- [9] K.-K. Wong and K.-F. Tong, "Fluid antenna multiple access," *IEEE Trans. Wireless Commun.*, vol. 21, no. 7, pp. 4801–4815, Jul. 2021.
- [10] L. Zhu, W. Ma, and R. Zhang, "Movable-antenna array enhanced beamforming: Achieving full array gain with null steering," *IEEE Commun. Lett.*, vol. 27, no. 12, pp. 3340–3344, Dec. 2023.

- [11] K.-K. Wong, A. Shojaefard, K.-F. Tong, and Y. Zhang, "Fluid antenna systems," *IEEE Trans. Wireless Commun.*, vol. 20, no. 3, pp. 1950–1962, Mar. 2020.
- [12] K. K. Wong, A. Shojaefard, K.-F. Tong, and Y. Zhang, "Performance limits of fluid antenna systems," *IEEE Commun. Lett.*, vol. 24, no. 11, pp. 2469–2472, Nov. 2020.
- [13] P. Mukherjee, C. Psomas, and I. Krikidis, "On the level crossing rate of fluid antenna systems," in *Proc. IEEE Int. Workshop Signal Process. Adv. Wireless Commun. (SPAWC)*, Jul. 2022, pp. 1–5.
- [14] L. Tlebaldiyeva, G. Nauryzbayev, S. Arzykulov, A. Eltawil, and T. Tsiftsis, "Enhancing QoS through fluid antenna systems over correlated nakagami-m fading channels," in *Proc. IEEE Wireless Commun. Netw. Conf. (WCNC)*. IEEE, Apr. 2022, pp. 78–83.
- [15] C. Skouroumounis and I. Krikidis, "Fluid antenna with linear MMSE channel estimation for large-scale cellular networks," *IEEE Trans. Commun.*, vol. 71, no. 2, pp. 1112–1125, Feb. 2022.
- [16] X. Lai, T. Wu, J. Yao, C. Pan, M. El-kashlan, and K.-K. Wong, "On performance of fluid antenna system using maximum ratio combining," *IEEE Commun. Lett.*, vol. 28, no. 2, pp. 402–406, Feb. 2024.
- [17] C. Psomas and I. Krikidis, "Switched combining for reconfigurable fluid antenna systems," in *Proc. IEEE Int. Workshop Signal Process. Adv. Wireless Commun. (SPAWC)*, Sep. 2024, pp. 281–285.
- [18] L. Zhu and K.-K. Wong, "Historical review of fluid antenna and movable antenna," 2024, *arXiv:2401.02362*.
- [19] G. Hu, Q. Wu, D. Xu, K. Xu, J. Si, Y. Cai, and N. Al-Dhahir, "Movable antennas-assisted secure transmission without eavesdroppers' instantaneous CSI," *IEEE Trans. Mob. Comput.*, vol. 23, no. 12, pp. 14 263–14 279, Dec. 2024.
- [20] C. Wang, G. Li, H. Zhang, K.-K. Wong, Z. Li, D. W. K. Ng, and C.-B. Chae, "Fluid antenna system liberating multiuser MIMO for ISAC via deep reinforcement learning," *IEEE Trans. Wireless Commun.*, vol. 23, no. 9, pp. 10 879–10 894, Sep. 2024.
- [21] J. Zou, H. Xu, C. Wang, L. Xu, S. Sun, K. Meng, C. Masouros, and K.-K. Wong, "Shifting the ISAC trade-off with fluid antenna systems," *IEEE Wireless Commun. Lett.*, vol. 13, no. 12, pp. 3479–3483, Dec. 2024.
- [22] F. R. Ghadi, K.-K. Wong, W. K. New, H. Xu, R. Murch, and Y. Zhang, "On performance of RIS-aided fluid antenna systems," *IEEE Wireless Commun. Lett.*, vol. 13, no. 8, pp. 2175–2179, Aug. 2024.
- [23] W. K. New, K.-K. Wong, H. Xu, K.-F. Tong, and C.-B. Chae, "An information-theoretic characterization of MIMO-FAS: Optimization, diversity-multiplexing tradeoff and q-outage capacity," *IEEE Transactions on Wireless Communications*, vol. 23, no. 6, pp. 5541–5556, Jun. 2023.
- [24] W. Ma, L. Zhu, and R. Zhang, "MIMO capacity characterization for movable antenna systems," *IEEE Trans. Wireless Commun.*, vol. 23, no. 4, pp. 3392–3407, Apr. 2023.
- [25] L. Zhu, W. Ma, B. Ning, and R. Zhang, "Movable-antenna enhanced multiuser communication via antenna position optimization," *IEEE Trans. Wireless Commun.*, vol. 23, no. 7, pp. 7214–7229, Jul. 2024.
- [26] Z. Xiao, X. Pi, L. Zhu, X.-G. Xia, and R. Zhang, "Multiuser communications with movable-antenna base station: Joint antenna positioning, receive combining, and power control," *IEEE Trans. Wireless Commun.*, vol. 23, no. 12, pp. 19 744–19 759, Dec. 2024.
- [27] M. Olyaei and S. Buzzi, "User-centric cell-free massive MIMO with access points empowered by fluid antennas," in *Proc. IEEE Int. Workshop Signal Process. Adv. Wireless Commun. (SPAWC)*, Sep. 2024, pp. 666–670.
- [28] W. Ma, L. Zhu, and R. Zhang, "Compressed sensing based channel estimation for movable antenna communications," *IEEE Commun. Lett.*, vol. 27, no. 10, pp. 2747–2751, Oct. 2023.
- [29] J. Zhu, G. Chen, P. Gao, P. Xiao, Z. Lin, and A. Quddus, "Index modulation for fluid antenna-assisted MIMO communications: System design and performance analysis," *IEEE Trans. Wireless Commun.*, vol. 23, no. 8, pp. 9701–9713, Aug. 2024.
- [30] X. Chen, B. Feng, Y. Wu, D. W. K. Ng, and R. Schober, "Joint beamforming and antenna movement design for moveable antenna systems based on statistical CSI," in *Proc. GLOBECOM IEEE Global Commun. Conf.*, 2023, pp. 4387–4392.
- [31] Y. Ye, L. You, J. Wang, H. Xu, K.-K. Wong, and X. Gao, "Fluid antenna-assisted MIMO transmission exploiting statistical csi," *IEEE Commun. Lett.*, vol. 28, no. 1, pp. 223–227, Jan. 2024.
- [32] Z. Zheng, Q. Wu, W. Chen, and G. Hu, "Two-timescale design for movable antennas enabled-multiuser MIMO systems," 2024, *arXiv:2410.05912*.
- [33] X. Zeng, J. Fang, B. Wang, B. Ning, and H. Li, "Csi-free position optimization for movable antenna communication systems: A derivative-free optimization approach," *IEEE Wireless Commun. Lett.*, vol. 14, no. 1, pp. 53–57, Jan. 2025.
- [34] T. X. Doan, C. D. Ho, and H. Q. Ngo, "Massive MIMO under multi-keyhole channels: Does the use-and-then-forget bounding technique work?" *Phys. Commun.*, vol. 47, p. 101384, Aug. 2021.
- [35] P. Gu, S. Tian, and Y. Chen, "Iterative learning control based on nesterov accelerated gradient method," *IEEE Access*, vol. 7, pp. 115 836–115 842, 2019.
- [36] L. Xingsi, "An entropy-based aggregate method for minimax optimization," *Eng. Optim.*, vol. 18, no. 4, pp. 277–285, Aug. 1992.
- [37] S. M. Kay, *Fundamentals of statistical signal processing: estimation theory*. Prentice-Hall, Inc., 1993.